MODELING OF OZONE FORMATION AT A RURAL SITE IN SOUTHERN ONTARIO

D. A. PLUMMER, J. C. McCONNELL, P. B. SHEPSON, D. R. HASTIE and H. NIKI†

Centre for Atmospheric Chemistry, York University, North York, Ont. M3J 1P3, Canada and Centre for Research in Earth and Space Science, York University, North York, Ont. M3J 1P3, Canada

Abstract—A one-dimensional time-dependent photochemical diffusion model has been used to simulate the chemical and vertical transport processes occurring at a rural location within Southern Ontario. The model output has been compared with the extensive measurements of several atmospheric trace gases which were made at a rural site in Southern Ontario as part of SONTOS (Southern Ontario Oxidant Study) during the summer of 1992. In particular, the measurements include various VOCs, odd nitrogen components and RO_x which have been explicitly included in the model. For the case examined, observations at the site are typical of unpolluted background conditions and the model is able to reproduce the observed variation of many of the key trace gas species observed. Though the site is remote from large population centers there appear to be important local emissions of NO_x and non-methane hydrocarbons (NMHC). Modelling results suggest that for the day studied approximately 10 ppb of ozone was photochemically produced, and that the production of ozone was limited by the availability of NO_x ($NO + NO_2$). At the observed levels isoprene does not play a major role in the production of ozone. A comparison of observations and model calculations for peroxy radical and HNO_4 concentrations indicate a disagreement between the model and measurements.

Key word index: Tropospheric ozone, modelling, rural oxidants, Ontario.

INTRODUCTION

High concentrations of O_3 and other photochemically produced oxidants are recognized as having negative effects on the health of people, crops, and forests (Taylor, 1969; Heck *et al.*, 1984). A reduction of ozone concentrations in the U.S. by 40% has been estimated to yield a savings or surplus of 2.5 billion U.S. dollars due to increased production of crops such as corn and soybean (Heck *et al.*, 1988) In Ontario high levels of ozone above the Federal Standard have an associated annual cost of about $45 M (MOE, 1989) in terms of crop loss, not to mention human and animal health effects. Southern Ontario is both the most densely populated region of Canada and the region where the Canadian National Ambient Air Quality acceptable concentration of O_3 (82 ppb) is exceeded most frequently (CCME, 1991). The combination of large population and high levels of O_3 make understanding the processes behind the formation of O_3 in southern Ontario important. In order to further our knowledge of oxidant chemistry in this region of Canada the Southern Ontario Oxidants Study (SONTOS) was initiated.

As part of SONTOS an extensively instrumented measurement site was set up at a rural location near Hastings, Ont., within the Windsor–Quebec City Corridor, a heavily populated region of Canada running from the city of Windsor northeast to Quebec city. Measurements of trace gases, including NO, NO_2, NO_y (total reactive nitrogen), PAN, O_3, C_3–C_{10} hydrocarbons including isoprene, aldehydes and ketones, CO, and several species of organic nitrates, were conducted during the summer of 1992 and again during the summer of 1993 (Arias *et al.*, 1994; Hastie *et al.*, 1994; Niki, 1993; Roussel *et al.*, 1994; O'Brien *et al.*, 1994). A full description of the project is given by Reid *et al.* (1994). This paper details the use of a one-dimensional photochemical model to study local chemistry taking place at the measurement site under unpolluted conditions ($NO_x < 1$ ppb and $O_3 < 45$ ppb).

Biogenic hydrocarbons, and isoprene in particular, can play an important role in the photochemical production of ozone (Trainer *et al.*, 1987). However, isoprene concentrations measured during the course of this study rarely exceeded 1 ppb, and for the case modelled in this paper isoprene concentrations were not observed to rise above 0.3 ppb. In this study the effects of low concentrations of isoprene on local scale photochemistry are investigated.

† Deceased 1 April 1995.

Isoprene can be expected to significantly contribute to ozone generation only under conditions of favorable NO_x/NMHC ratios (Lurmann *et al.*, 1983). Since O_3 production over rural areas, with NO_x levels below a few ppb, are generally believed to be limited by the amount of NO_x present (Liu *et al.*, 1987), local sources of NO_x will strongly influence the local photochemical generation of ozone. Studies of the NO_x flux from soil have shown that over rural areas these emissions may be as large as local anthropogenic sources (e.g. Shepherd *et al.*, 1991). Without direct measurements of the flux of NO_x from the soil the modelling study presented here cannot conclusively deduce the importance of soil NO_x emission relative to combustion sources. However, model results do indicate local sources of NO_x are necessary to explain the observed concentrations and that the emission of NO_x from soil may represent a large fraction of the local NO_x emission.

During daylight periods the reaction of NO with O_3 forming NO_2 and the subsequent photolysis of NO_2 producing NO and O_3,

$$NO + O_3 \rightarrow NO_2 + O_2 \quad (1)$$

$$NO_2 + h\nu \xrightarrow{O_2} NO + O_3 \quad (2)$$

form a fast photochemical system that is near steady state. Peroxy radicals, from the atmospheric oxidation of hydrocarbons, will oxidize NO as well. The presence of peroxy radicals will perturb the NO_x–O_3 system and lead to a photochemical generation of ozone (Parrish *et al.*, 1986). Peroxy radicals may also react with themselves and with other peroxy radicals. Such reactions will not result in the production of ozone and will become increasingly important under low NO_x conditions. Direct measurements of peroxy radical concentrations were made at the Hastings site using a chemical amplifier technique (Arias *et al.*, 1994). Since peroxy radicals are extremely short lived they are little affected by horizontal transport and therefore ideally suited for study with a one-dimensional model. A direct comparison between model calculations and observations of peroxy radicals will provide an important test of our understanding of tropospheric photochemistry at the site.

In addition to the generation of O_3, the reaction of NO with a peroxy radical may result in the addition of the NO resulting in the formation of an organic nitrate,

$$RO_2 + NO \longrightarrow \alpha RONO_2 + (1-\alpha)(RO\cdot + NO_2) \quad (3)$$

where α is the organic nitrate yield. The formation of organic nitrates impact both the radical and NO_x cycles (Carter and Atkinson, 1989) and organic nitrates may constitute a significant fraction of the total reactive nitrogen, NO_y (O'Brien *et al.*, 1994). For alkanes the organic nitrate yield is relatively well known and has been shown to increase with increasing hydrocarbon molecular weight (Atkinson, 1990). The formation of hydroxyalkyl nitrates, through the oxidation of alkenes, is not as well understood, but it is generally believed that the nitrate yields for hydroxyalkyl peroxy radicals are lower than that for the corresponding alkyl peroxy radicals (Atkinson, 1990). Various alkyl and hydroxyalkyl nitrates were measured at the Hastings site (O'Brien *et al.*, 1994) and model calculations are compared with observations.

The work presented here focuses on observations made on the date of 6 August 1992. Much of the day was characterized by trace gas variations that are typical of "unpolluted" background conditions at this site. For the early part of the day the winds were from the west (Fig. 3c in Reid *et al.*, 1994). Around noon (EDT) the winds veered to the northwest and then backed to the west around 1500 EDT. The wind continued to back and at roughly 1730 EDT the concentration of many of the trace gases and meteorological variables measured at the site were observed to change rapidly (cf. Fig. 2 of Reid *et al.*, 1994). Ozone concentrations increased from 42 to 68 ppb within 15 min and total odd nitrogen (NO_y) levels increased from 1.2 to 6.8 ppb during the same period. It is likely that this dramatic change in the air mass is due to a polluted plume of air that left Toronto early in the morning of 6 August. Simple geostrophic forward trajectories from Toronto on 6 August suggest that the plume travelled out over Lake Ontario, carried along by prevailing westerly winds. In the afternoon the geostrophic wind became more southwesterly. The change in wind direction, coupled with an existing land-lake breeze, transported the polluted air mass inland toward the Hastings site.

Because of the impact of the putative Toronto plume, modelling has been restricted to observations made at the site prior to the arrival of the polluted air mass in an effort to gain a greater understanding of the background conditions at this site. The variation in concentration of the major trace gases observed at the site during the "clean air" portion of 6 August are typical of the variations observed during other clean air days at this site and we therefore feel that the conclusions derived from the modelling study of 6 August 1992 apply broadly to background conditions at this site. Simple two-day geostrophic back trajectories from Hastings also suggest that the air had not passed over Toronto. However, during the middle of the day when the wind was veering there may have been some contribution from Peterborough, a town of approximately 65,000 inhabitants 40 km to the NW.

SITE DESCRIPTION

The Hastings field site is located in southern Ontario about 40 km north of Lake Ontario and about 130 km northeast of metropolitan Toronto, and urban area with a population of over 3 million people. The nearest settlement to the site is the town of Hastings (population 1000), 4 km to the southwest. The area within 1 km of the measurement site is predominantly farmland with heavily forested woodlots. An analysis by Ontario Hydro (Roussel and

Moroz, 1992) indicated no significant point sources for hydrocarbons or NO_x near the site. As such, the air chemistry at the site is dominated by relatively clean continental background conditions ($NO_x < 1$ ppb and $O_3 < 40$ ppb), however, the site is frequently affected by the transport of polluted air from Toronto and the surrounding area when the winds are from the southwest (Roussel and Moroz, 1992).

The main measurement site sits atop a hill that is 28 m above the Trent river, approximately 250 m to the north. There is a second measurement site, for meteorological variables, located at the bottom of the hill. The behavior of trace gases at the site during times when a stable nocturnal boundary layer is present is complicated by local dynamical effects. If the nocturnal boundary layer (NBL) is stable, preventing upslope flow, the air flow may actually be around the hill, with the resultant disconnection of the site from the surrounding area and local surface sources. Alternatively, cold air drainage down the sides of the hill at night can occur, again effectively decoupling the air at the site from the surface. This will influence the trace gas behavior that is inferred from the measurements. Those species subject to removal by dry deposition or emitted at the surface will be particularly influenced by the local air flow. A one-dimensional model could not be expected to account for these influences. Therefore the model description of the nocturnal chemistry will be relatively more qualitative.

MODEL DESCRIPTION

The time evolution of the mixing ratio for all trace gases within the model is given by the simplified continuity equation

$$\partial f_i/\partial t + \partial \Phi_i/M\,\partial z = P_i/M - L_i f_i \qquad (4)$$

where f_i is the mixing ratio of the species, M (cm^{-3}) is the background number density, P_i ($cm^{-3}\,s^{-1}$) is the production rate of species i and L_i (s^{-1}) is the loss frequency. The vertical flux, $\Phi_i = -K_z M\,\partial f_i/\partial z$ and K_z ($cm^2\,s^{-1}$) is the vertical eddy diffusion coefficient.

The continuity equation is solved for all species using an operator splitting technique, where the vertical diffusion and chemistry terms are solved separately for a non-uniform grid. Fluxes into or out of the model, including emissions and dry deposition, are treated as part of the chemistry term. The chemistry portion of the continuity equation is solved using a completely implicit scheme with a Newton's method solver, which is mass conserving (e.g. McConnell *et al.*, 1991). The diffusion operator is solved by a second-order finite difference method which is not mass conservative. However, conservation is strictly enforced for the diffusion operator by scaling the mixing ratios of each species, uniformly at all heights, at each time step in order to conserve the total column mass. A timestep of 15 min has been used for convenience and speed as it is not essential for this analysis to resolve the details of the chemistry near sunrise or sunset.

The deposition velocities used within the model are given in Table 1 while details of the emissions used in the model are described below. The top of the model is in the free troposphere at a height of 1.85 km and, on the time scales of a few days, we have assumed that the fluxes in and out of the upper boundary are zero. The bottom nine layers of the model stretch from 3 to 250 m with increasing spacing between layers. Above 250 m a constant spacing of 200 m is maintained up to 1.85 km.

The diurnal behavior of the planetary boundary layer is parameterized to reproduce the main features of a typical diurnal cycle as described in Stull (1988). At night K_z is fixed at $1.0 \times 10^3\ cm^2\,s^{-1}$ within the bottom 100 m. Between 100 m and the maximum height of the daytime mixed layer K_z is set to $1.0 \times 10^2\ cm^2\,s^{-1}$, to simulate a residual layer. The nighttime profile for K_z is maintained until 830 EDT to reproduce the observed variation of the boundary layer as evidenced by the behavior of O_3 and other trace gases that are strongly depleted from within the NBL. The behavior of the boundary layer during the daytime is parameterized using the time-dependent function for K_z and the height of the planetary boundary layer given by Singh *et al.* (1993). The original function for K_z given by Singh *et al.* is independent of height and is modified for the purpose of this paper to include an exponential height dependence for K_z. The height of the mixed layer increases from 100 m at 830 EDT to a maximum height of 1.25 km at 1200 EDT. Above 1.25 km K_z is kept constant at $1.0 \times 10^4\ cm^2\,s^{-1}$. The eddy diffusion coefficient switches from a daytime well mixed profile to a stable nighttime profile at 1930 EDT, about one hour before sunset.

The model run is started at midnight of 6 August and continued for 24 h. The surface initial conditions

Table 1. Species deposition velocities ($cm\,s^{-1}$) used in the clean air case

Species	V_d ($cm\,s^{-1}$)
O_3	0.3[a]
NO_2	0.2
HNO_3	1.0
H_2O_2	0.6
HCHO	0.75
ALD_2	0.75
PAN and PAN analogs	0.60[a]
HAC	0.75
HNIT	1.0
ISONIT	1.0
MVKNIT	1.0
MACNIT	1.0

ALD_2, C_2 and greater aldehyde; HAC, hydroxyacetyladehyde; HNIT, hydroxyalkyl nitrate; ISONIT, isoprene nitrate: MVKNIT, methyl vinyl ketone nitrate; MACNIT, methacrolein nitrate.

[a]Hastie *et al.* (1993).

for NO_x, ozone, and CO are based on the measurements (cf. Reid *et al.*, 1994). Since there are no measurements relating to the variation of the species with height, as required by the model, we have used the measurements taken at 1000 EDT as approximate indicators of the nighttime mixing ratios in the residual layer above the NBL. This is particularly the case for O_3 and NO_x. For the alkanes and alkenes we have assumed that the early morning measurements can be applied to the midnight starting values and also that these same conditions are independent of height. The initial concentration of nitric acid and all of the organic nitrate species are assumed to be zero. The initial concentrations of the short-lived species e.g. PAN, HCHO, isoprene and many of its oxidation products, are derived from a five-day initialization run performed using identical boundary conditions as those used in the standard model run.

CHEMICAL MECHANISM

The chemical reaction mechanism used in the model is largely based on the work of Lurmann *et al.* (1986), with the additions suggested by Jacob and Wofsy (1988). The reaction

$$OH + HO_2 \rightarrow H_2O + O_2 \qquad (5)$$

has been added to the original mechanism, as has a more complete treatment of organic nitrates. The loss of organic nitrates by photolysis and reaction with OH has been added. All loss mechanisms for organic nitrates are assumed to yield stable products. For isoprene the organic nitrate yield has been set to 12% (Tuazon and Atkinson, 1990). The reaction of OH with the isoprene derived nitrate is assumed to occur at the same rate as OH attack on the lumped alkene species used within the mechanism ($4.1 \times 10^{-12} e^{537/T}$). This assumption is reasonable given that the isoprene nitrate will still contain a carbon–carbon double bond.

The model calculates the photolysis rates allowing for Rayleigh scattering, O_3 absorption, and a surface albedo using the approach of Henderson *et al.* (1990). The surface albedo was set to 0.15 and the total column ozone was 310 Dobson units. The photolysis reactions and model calculated local noon J-values are given in Table 2.

The non-methane hydrocarbons are treated using both a lumped molecule and surrogate species approach. The C_3, smaller alkanes and ethene are treated explicitly within the mechanism. The C_4 and larger alkanes are lumped together as one hydrocarbon while the C_3 and larger alkenes are treated as the surrogate propene-like alkene. Formaldehyde is treated separately though higher aldehydes, except methacrolein, are lumped together as a single aldehyde species. With the exception of methyl vinyl ketone all ketones are lumped together as one species.

EMISSIONS

Emissions of NO_x into the model have been separated into two components: a constant flux, meant to be representative of the emission of NO_x from the soil, and a diurnally varying anthropogenic flux. For the latter, we have used as a template the temporal behavior of the NO anthropogenic flux taken from the Acid

Table 2. Rates for 6 August 1300 EDT, at 1 km elevation, clear sky conditions and SZA = 27°

Photolysis reaction	Rate (s^{-1})
1. $NO_2 + h\nu \rightarrow NO + O_3$	1.22×10^{-2}
2. $NO_3 + h\nu \rightarrow 0.15(NO + O_2)\ 0.85(NO_2 + O_3)$	4.01×10^{-1}
3. $O_3 + h\nu \rightarrow O1D + O_2$	3.91×10^{-5}
4. $HONO + h\nu \rightarrow NO + OH$	2.72×10^{-3}
5. $HNO_3 + h\nu \rightarrow NO_3 + OH$	1.40×10^{-6}
6. $H_2O_2 + h\nu \rightarrow 2\,OH$	1.10×10^{-5}
7. $HNO_4 + h\nu \rightarrow NO_2 + HO_2$	6.84×10^{-6}
8. $HCHO + h\nu \rightarrow 2HO_2 + CO$	4.34×10^{-5}
9. $HCHO + h\nu \rightarrow CO + H_2$	3.51×10^{-5}
10. $ALD_2 + h\nu \rightarrow MO_2 + HO_2 + CO$	4.84×10^{-6}
11. $ALD_2 + h\nu \rightarrow CH_4 + CO$	3.12×10^{-7}
12. $KET + h\nu \rightarrow MCO_3 + ETO_2 + H_2O$	1.01×10^{-6}
13. $GLYX + h\nu \rightarrow PROD$	9.76×10^{-5}
14. $MGLY + h\nu \rightarrow MCO_3 + HO_2 + CO$	2.32×10^{-5}
15. $DIAL + h\nu \rightarrow 0.98\,HO_2 + 0.02\ MCO_3 + TCO_3$	1.35×10^{-5}
16. $HAC + h\nu \rightarrow HCHO + HO_2$	1.35×10^{-5}
17. $MGGY + h\nu \rightarrow MCO_3 + HO_2$	1.35×10^{-5}
18. $RONO_2 + h\nu \rightarrow PROD$	1.22×10^{-6}

ALD_2, C_2 and greater aldehydes; MO_2, CH_3O_2; KET, lumped ketone; MCO_3, CH_3COO_2; ETO_2, $C_2H_5O_2$; GLYX, glyoxal; PROD, stable product; MGLY, methyl glyoxal; DIAL, dicarbonyl; TCO_3, CHOCH $= CHCO_3$; HAC, hydroxyacetyladehyde; MGGY, α-dicarbonyl; $RONO_2$, organic nitrates.

Deposition and Oxidants Model, a regional scale model used by the Ontario Ministry of the Environment (Wong, 1993). Scaling the emission to match the midday NO_x measurements, we obtain a peak NO flux of 3.0×10^{10} molecules $cm^{-2} s^{-1}$ at 1400 EDT. The average NO flux over the day is 1.7×10^{10} molecules $cm^{-2} s^{-1}$, which is within the range of NO_x emission rates reported by the Ontario Ministry of the Environment in a 1987 emissions inventory for the Hastings area (Roussel and Moroz, 1992). Figure 1 indicates the standard NO flux that was used in the model. This emission profile does not yield a sufficiently large input during the nighttime period and we have thus added a constant NO flux of 1.5×10^{10} molecules $cm^{-2} s^{-1}$ into the bottom layer of the model. We rationalize this second flux by assuming that it may be as a result of emission of NO from the soil. The magnitude of the flux is within the range of soil NO_x emission rates reported for southern Ontario (e.g. Shepherd *et al.*, 1991). The soil NO flux is emitted into the bottom layer of the model while the anthropogenic component of the NO flux is spread evenly over the bottom 100 m of the model. This spreading is to simulate mixing that will take place before the NO_x reaches the site. During the day the exact height range over which the NO flux is mixed is less important due to the rapid rate of vertical mixing. At night the flux is contained within the NBL as would be expected of local emissions beneath a strong inversion.

Emissions of anthropogenic hydrocarbons are scaled to the anthropogenic NO flux and applied equally over the bottom 100 m of the model in the same way as NO_x emissions. The emission of hydrocarbons, as a fraction of NO_x emissions (mol/mol), were as follows: C_2H_6, 0.24; C_3H_8, 0.16; C_4 alkane, 0.50; C_2H_4, 0.09; propene, 0.60; aromatic hydrocarbons, 0.06. These hydrocarbon/NO_x ratios were taken from aircraft borne simultaneous measurements of NO_x and hydrocarbons above Toronto (McLaren *et al.*, 1994). The one exception was propene which was measured as 0.09 NO_x during the aircraft flight. Using the measured hydrocarbon to NO_x emission ratio for propene, the model greatly under predicted the observed concentration of propene, and a propene emission equivalent to 0.60 NO_x was necessary to give reasonable agreement between model predictions and observations. The total emission of anthropogenic hydrocarbons used in the model was 6.0 ppb C/ppb NO_x by volume.

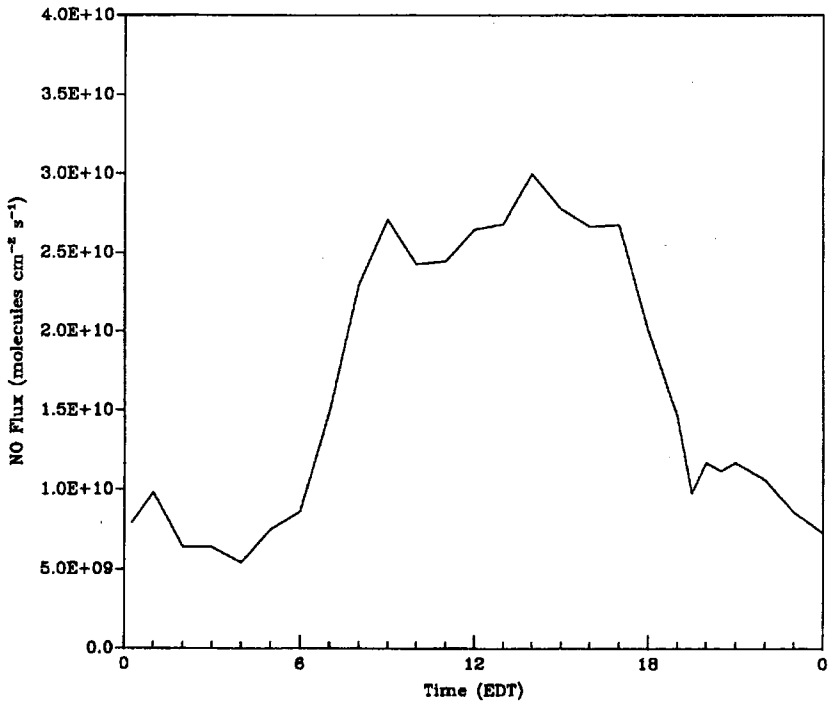

Fig. 1. The standard diurnal anthropogenic NO flux used in the model and input into the bottom 100 m. The details are given in the text.

Previous studies have shown that isoprene is often the dominant non-methane hydrocarbon involved in the local photochemical production of O_3 at rural sites (e.g. Trainer *et al.*, 1987). In this model, to describe the emission of isoprene from vegetation, we adopt the expression of Guenther *et al.* (1993) for isoprene emission from a single leaf. This expression is then extrapolated to a canopy following the approach of Jacob and Wofsy (1988). The emission of isoprene predicted by the model begins to saturate with respect to light levels between 400 and 600 μmol cm^{-2} s^{-1}; a light level which is attained relatively early in the morning. Thus for our conditions isoprene will be controlled by temperature for most of the day. For the clean air simulation of 6 August 1992 the model isoprene flux peaks at 3:00 PM EDT and 25°C at 7.1×10^{10} molecules cm^{-2} s^{-1}. This value represents an average emission over the farmland and woodlots surrounding the site. As the magnitude of the isoprene emission used in the model has been scaled to reproduce the observed concentration of isoprene, the rate of isoprene emission will be sensitive to the values of K_z used. Larger values of K_z would result in a faster rate of transport of isoprene away from the surface and, consequently, a larger rate of isoprene emission would be required to achieve the same near surface isoprene concentration. The emission of isoprene was distributed evenly over the lowest 11 m of the model. The temporal variation of the model isoprene emission and the observed temperature are shown in Fig. 2.

RESULTS AND DISCUSSION

As noted above the focus of this study is on the understanding of background chemistry conditions at the Hastings site, and the behavior of the short-lived species in particular. Here we present a comparison between model calculations and observations for several of the important trace gas species.

NO *and* NO_2

In Fig. 3 we present the diel behavior for NO, NO_2, NO_x, HNO_3, NO_y, and the NO_x/NO_y ratio from the model together with the measurements of Roussel *et al.* (1994) and Hastie *et al.* (1994) for 6 August. As noted above, the behavior of NO and NO_2 at night is complicated by local dynamical effects. However, the model is still able to reproduce the major features of the variation. During the nighttime the fraction of NO_y in the form of NO_x is greater than 70%. A large

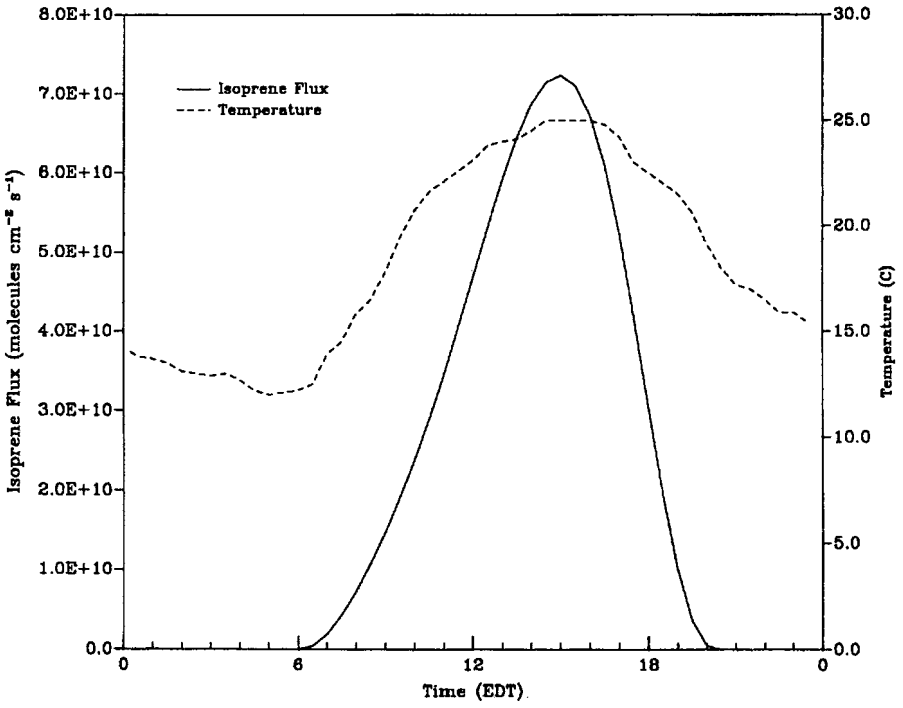

Fig. 2. The standard isoprene flux into the bottom 11 m of the model (solid line) and the observed near surface temperature.

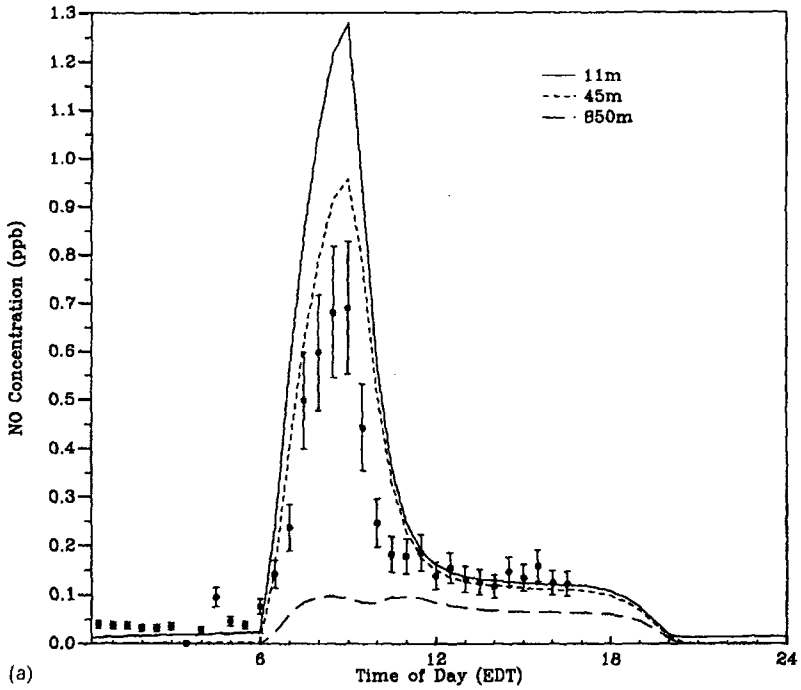

(a)

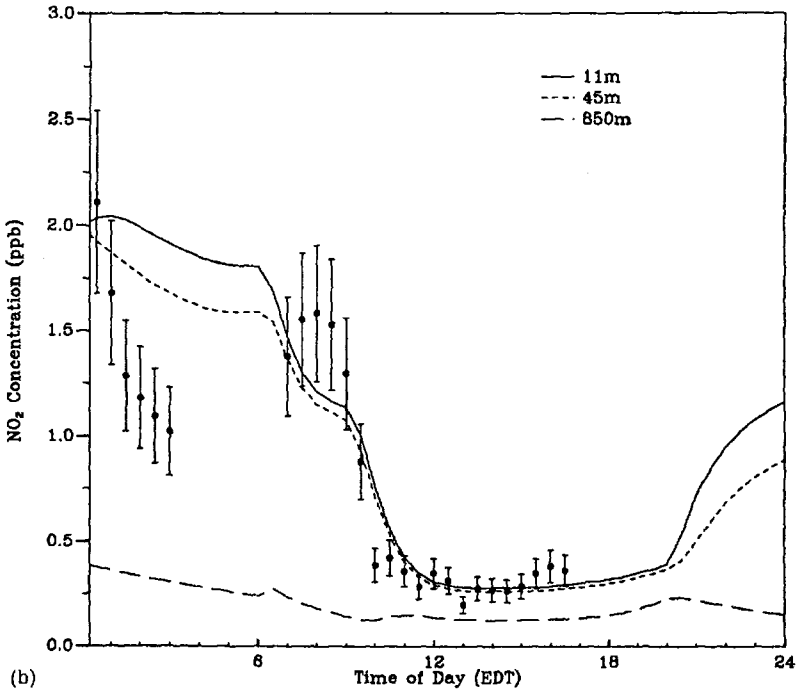

(b)

Fig. 3a and b.

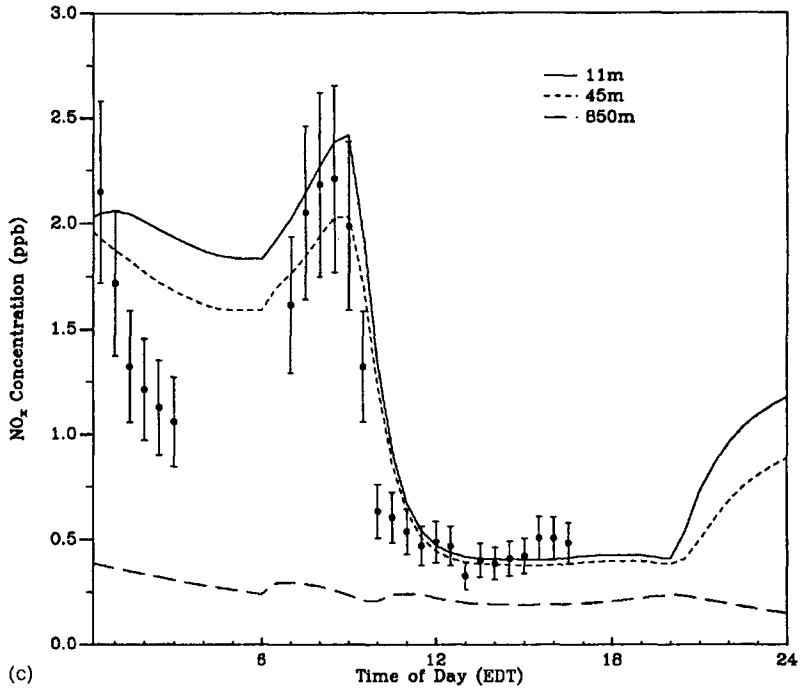

(c)

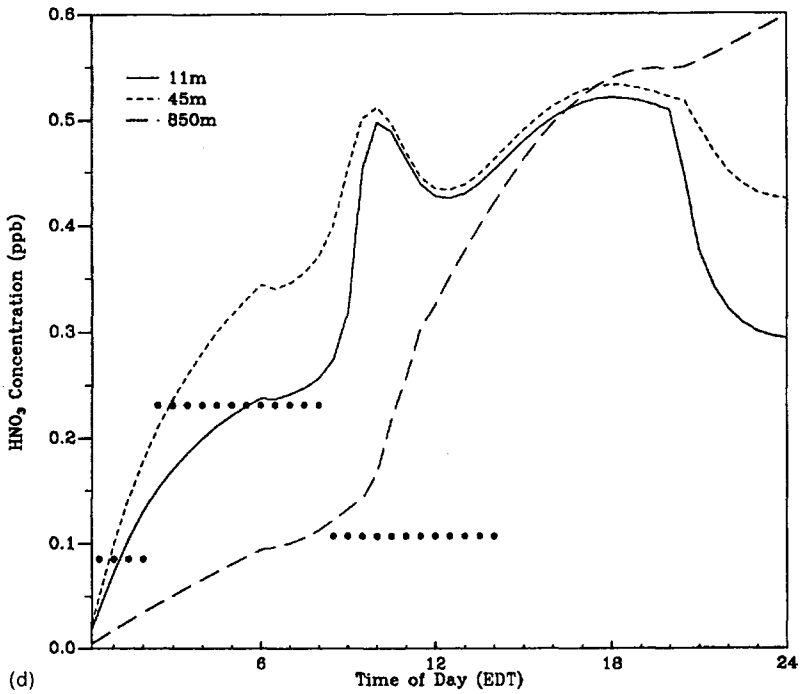

(d)

Fig. 3c and d.

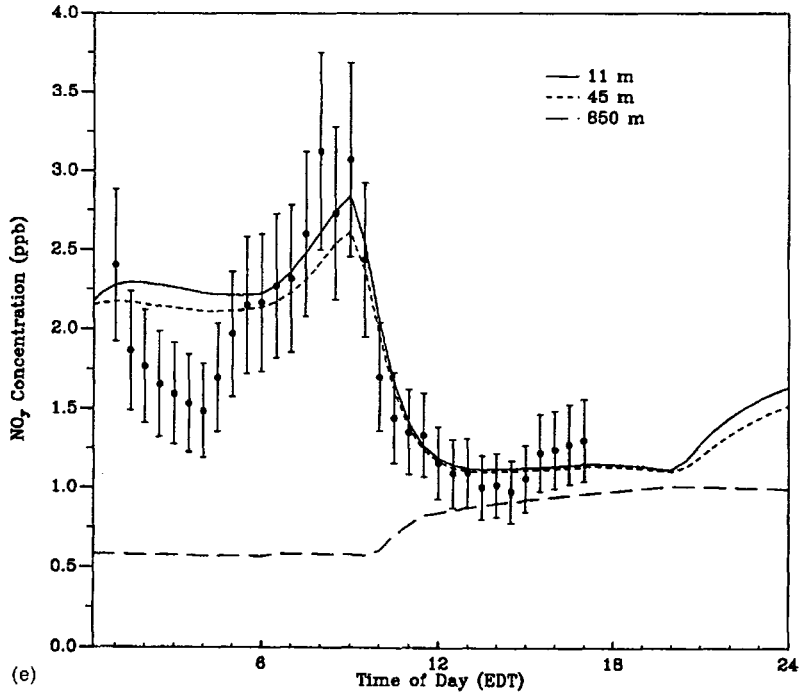

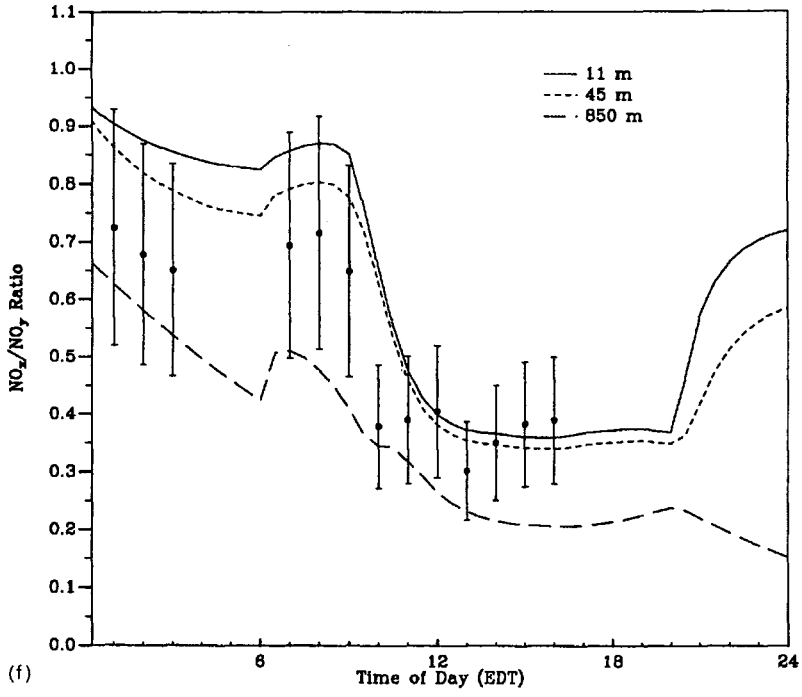

Fig. 3. The diurnal variation of model mixing ratios for several nitrogen species at 11, 45, and 850 m. (a) NO, (b) NO_2, (c) NO_x, (d) HNO_3, (e) NO_y and (f) NO_x/NO_y. The measurements are also shown for NO, NO_2, NO_x (Hastie *et al.*, 1994); NO_y (Roussel *et al.*, 1994); and HNO_3 (Reid *et al.*, 1994).

fraction of NO_y as NO_x indicates that the NO_x has not undergone a great deal of photochemical processing since the time of emission, and suggests the sources of the NO_x being observed at night are of local origin. It is noteworthy that to maintain a NO_2 abundance of approximately 1 ppbv in the NBL (Fig. 3b) a surface emission of $\sim 1 \times 10^{10}$ molecules $cm^{-2} s^{-1}$ is required. Since this is typical of emission rates from soils (e.g. Shepherd *et al.*, 1991), we believe that at night the dominant source of NO_x is from the soil. Once the NO is emitted it is quickly oxidized to NO_2 by reaction with O_3. The NO_2 produced, is removed from the NBL both directly and indirectly: directly by dry deposition (with a time constant of ~ 14 h) and indirectly by conversion of NO_2 to N_2O_5 (rate limited by the conversion to NO_3 with a time constant ~ 6 h), followed by the heterogeneous reaction of N_2O_5 with liquid water to form HNO_3 which then deposits. The result of the soil NO flux is an increase in NO_y within the NBL. The actual observations are much more complex reflecting local micrometerological effects as discussed above. NO_x concentrations, which were greater than 2 ppb at midnight of 6 August, drop rapidly to nearly 1 ppb within 3 h. The model is unable to reproduce this feature using chemical and reasonable deposition losses for NO_x. At night the dominant source of NO_x will be emission from the soil, and with slow vertical mixing NO_x can be expected to possess a strong vertical gradient, with concentration dropping rapidly with height. Such a feature is predicted by the model (Fig. 4). If, as hypothesized, between 000 and 300 EDT the air sampled at the hilltop measurement site originated above the surrounding countryside, the concentrations of NO_x within this air would have been considerably lower than in air originating closer to the surface. The decoupling of air at the measurement site from the surface may be responsible for the rapid decrease in NO_x concentrations between 000 and 300 EDT, though a change in air mass cannot be ruled out.

At sunrise photolysis of NO_2 leads to a rapid increase in NO concentrations (Fig. 3a), as the NO_x remains trapped near the ground until the breakup of the nocturnal inversion (Fig. 3c). Between sunrise and the breakup of the nocturnal inversion NO_x concentrations are observed to increase at the surface. Model runs conducted with a constant soil NO flux and no anthropogenic flux gave a rise in NO_x, though both the magnitude of the increase and the halfwidth of the peak were much smaller than that observed. The increase in NO_x concentrations, despite a constant NO_x input, is related to the rate of NO_x loss by dry deposition. The fraction of NO_x present as NO_2 dur-

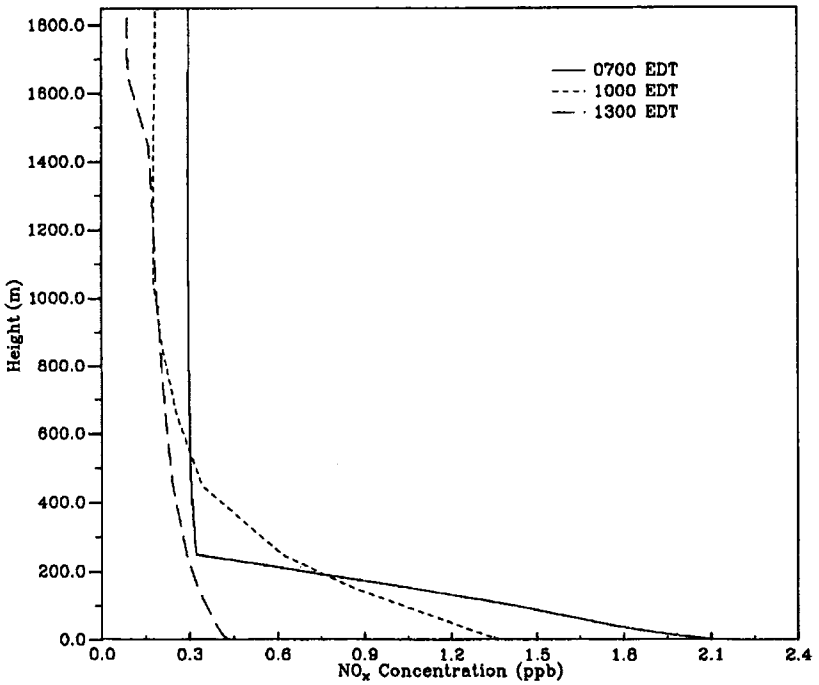

Fig. 4. Vertical distribution of NO_x at 0700, 1000, and 1300 EDT.

ing daylight periods will be comparatively smaller than the fraction of NO_x in the form of NO_2 during the nighttime periods. As a result, the rate of NO_x loss by dry deposition will decrease after sunrise. Observations indicate an increase in NO_x concentrations after sunrise nearly three times larger than that predicted by the model with only a constant NO_x flux. With the addition of a diurnally varying anthropogenic NO flux (Fig. 1), which increases in magnitude rapidly after 500 EDT, the model predicted rise in NO_x after sunrise is in much better agreement with observations.

At 900 EDT, with the breakup of the nocturnal inversion, the high concentrations of NO_x near the surface mix upward and are diluted with less NO_x rich air above. The result is a sharp decrease in NO and NO_2 concentrations in the lowest 100 m of the model after 900 EDT (cf. Fig. 3). The model predicted concentrations of NO and NO_2 follow observations made at the site on 6 August 1992 reasonably well until 1800 EDT, when the rapid change in air mass is observed to occur. Of course, the midday agreement is not too surprising since the surface emissions were adjusted to fit the daytime observations. However, our calculations do indicate that a source of anthropogenic NO_x is required to maintain the observed NO_x concentrations over the course of the day.

Figure 3d shows the model calculated gas phase HNO_3 mixing ratio vs time and the filter data of Reid *et al.* (1994) collected over six-hour integration periods. There is reasonable agreement during the early part of the morning, though the agreement during this time is due to the HNO_3 concentration used to initialize the model. By noon the model is overpredicting HNO_3 by more than a factor of three. At sunrise, 0600 EDT, the HNO_3 concentration, averaged over the bottom 1250 m of the model, is calculated to be 0.14 ppb. At 1400 EDT the nitric acid concentration is calculated to be approximately 0.45 ppb, averaged over the depth of the PBL. Therefore, it is clear that much of the NO_x conversion to HNO_3 is being calculated to occur during the daytime, predominately through the reaction of NO_2 with OH. It is possible that some of the HNO_3 that has been formed in the model should have been converted to NO_3^-, reducing the model HNO_3. To some extent this may be accounted for by adding the measured NO_3^- to the measured HNO_3. Even accounting for possible NO_3^- formation, there still remains considerable discrepancy between model predictions and observations of HNO_3 and NO_3^-. We do note, however, that serious problems are known to exist with the consistency of HNO_3 measurement at concentrations below 1 ppb (Crosley, 1994), and the possibility that the model does not adequately account for the loss of HNO_3 by dry deposition remains.

The total odd nitrogen, NO_y, calculated by the model and observed, is shown in Fig. 3e. There is reasonable agreement between model calculations and observations from 0600 until the end of the comparison at 1700 EDT. The agreement between the modelled and observed concentration of NO_y during the afternoon is surprising, given that the model appears to be overpredicting the concentration of HNO_3 during this time. Between the hours of 1300 and 1500 EDT the NO_y concentration is at its lowest value of the day and, at the same time, model agreement with the observed NO_y concentration is good. Looking more closely at the daytime partitioning of odd nitrogen, in particular for 1400 EDT and the 11 m grid point, the model predicts the following concentrations: NO_x, 0.41 ppb; HNO_3, 0.45 ppb; PAN, 0.15 ppb; and NO_y, 1.12 ppb. The species given above account for 90% of the total NO_y predicted by the model, with the remaining NO_y comprised of PAN analogues (3% NO_y), organic nitrates (6% NO_y), HONO, and HNO_4. Observations of the nitrogen species give the following concentrations: NO_x, 0.39 ppb; HNO_3, 0.11 ppb; NO_3^-, 0.09 ppb; PAN, 0.19 ppb; and NO_y, 1.02 ppb. Including the measured organic nitrates (see below), the measurements of the individual NO_y components fail to account for 0.24 ppb of the total measured NO_y. The inability to account for all of the measured NO_y by measurements of the component species has been observed before (Fahey *et al.*, 1986; Buhr *et al.*, 1990, for example). The measurements and the model agree quite well for NO_x, PAN, and total NO_y, while the model partitions the NO_y missing from the individual measurements as HNO_3. Given the known difficulties with HNO_3 measurements at concentrations below 1.0 ppb (Crosley, 1994), the model results suggest that the HNO_3 measurements are not capturing all of the HNO_3 present. At this point, however, the problem of the partitioning of NO_y remains unsolved and warrants continued attention.

Figure 3f shows the NO_x/NO_y ratio which, as previously mentioned, provides an important measure of the photochemical age of the air mass. Both the measurements and model indicate nighttime odd nitrogen was relatively "fresh". During the day the NO_x/NO_y ratio decreases indicating increased chemical oxidation. Overall, model calculations and observations of the NO_x/NO_y ratio are in good agreement over much of the day.

Isoprene

Figure 5 shows the modelled isoprene mixing ratios at 11, 45 and 850 m for the standard emission case. Also shown are the measurements taken at the site. The sharp rise in isoprene concentration predicted by the model just after dawn reflects the emission of isoprene into the shallow NBL. The rapid decrease in near surface concentration after 900 EDT reflects the break up of the NBL and the dilution of the isoprene emission into a greater volume. The fact the measurements do not show evidence of a sharp early morning peak in isoprene concentration may be related to the frequency of the measurements. The timing of the breakup of the nocturnal inversion within the model

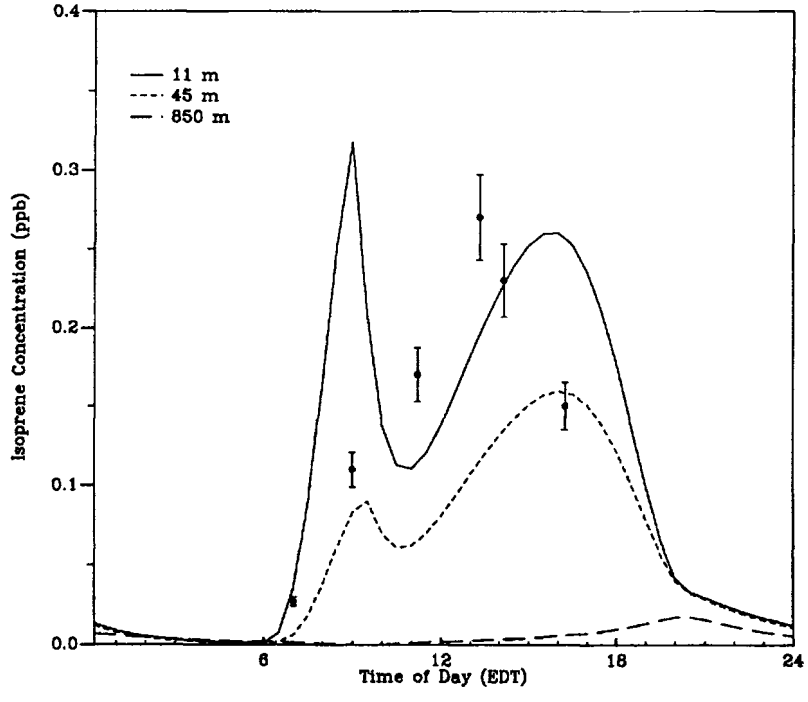

Fig. 5. Model calculated diurnal isoprene mixing ratio at 11, 45 and 850 m and surface measurements for the standard model run.

will also be critical to the development of the early morning peak in surface isoprene concentrations.

The midday peak isoprene concentration predicted by the model occurs late in the afternoon, about 3 h after the peak in the measurements. This is a reflection of the strong dependence of the model isoprene emission on temperature, which peaks around 1500 EDT (Fig. 2). Part of the reason for the disagreement in timing of the peak isoprene concentration may be due to the limited nature of a one-dimensional model. The model isoprene emission varies with temperature and light level but does not, because of the nature of a one-dimensional model, vary with location. Over the course of the day, the wind direction at Hastings was observed to change from the northwest to the southwest. The air arriving at the measurement site would have been exposed to different isoprene sources, with different emission strengths, as the wind direction changed, and this effect may partly account for the difference in timing between the observed peak isoprene concentration and that calculated by the model.

Ozone

The model predictions and the surface observations for O_3 are shown in Fig. 6. During the nighttime there is no detailed agreement: however, there is qualitative agreement given the limitations of the model's representation of the meteorological situation at the site. The measured O_3 remains elevated until about 0330 EDT, when it begins to decrease, while the model O_3 decreases throughout this period. Sounder acoustic data and vertical temperature gradients near the surface show evidence of a stable inversion over the site during the early morning hours of 6 August 1992. Thus, we would expect O_3 to deposit during the night with a concomitant decrease in mixing ratios within the NBL, as produced by the model and as observed, for example, in the measurements at Dorset, Ontario (Hastie *et al.*, 1993). Local micrometeorological effects, as noted above, obviously strongly impact the behavior of O_3 during the night.

After the early morning breakup of the nocturnal inversion, higher concentrations of O_3 from above the nocturnal inversion are mixed down to the surface. The result is a sharp rise in O_3 concentrations shortly after 900 EDT. As expected the model reproduces this feature well. During the remainder of the morning and into the middle of the afternoon the model and measured O_3 concentrations are in reasonable accord. Thus the rate of local photochemical O_3 production and transport calculated by the model closely matches

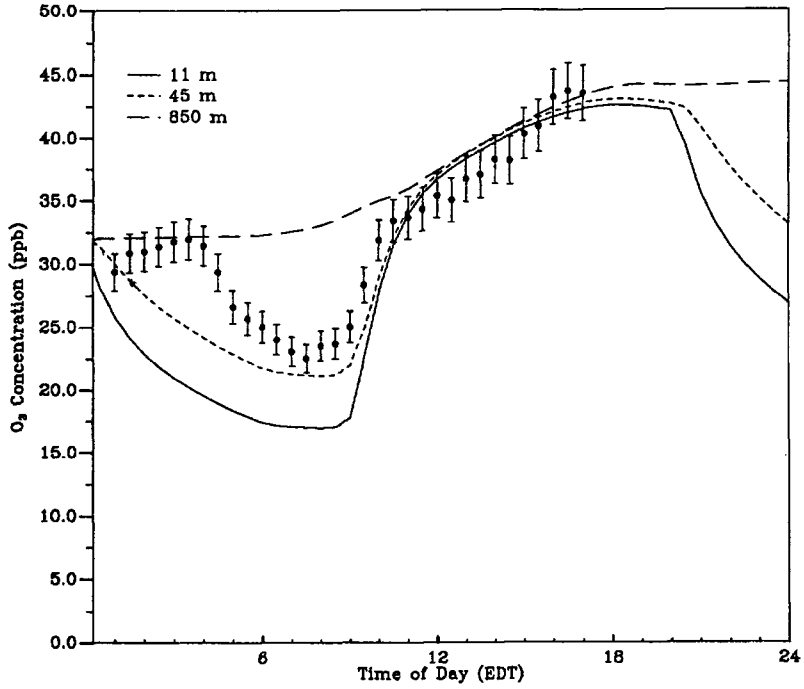

Fig. 6. Model calculated diurnal variation of O_3 at 11, 45, and 850 m. Also shown are the surface O_3 measurements (Hastie *et al.*, 1994; Roussel *et al.*, 1994).

that which was observed. After 1500 EDT the O_3 concentrations calculated by the model begins to level off while observations show O_3 concentrations increasing steadily until 1700 EDT (Fig. 6). A steady increase in concentration through the late afternoon hours is a typical feature of the diurnal variation of O_3 observed at this site. It is believed that the advection of higher concentrations of O_3, produced elsewhere, is responsible for the late afternoon rise in O_3 (Hastie *et al.*, 1996). Such an effect is also suggested by the observations of C_2Cl_4 (cf. Reid *et al.*, 1994), a distinctive tracer of anthropogenic air, which displayed a steady increase in concentration during the afternoon.

Ozone production

As noted above, during the day the dominant chemical source of O_3 is the oxidation of NO to NO_2 by peroxy radicals, as shown by reaction (3), followed by the photolysis of NO_2. Figure 7 shows the rate of O_3 production from the reaction of NO with HO_2 and several species of peroxy radicals at two model levels, 20 and 850 m. At both levels the main source of O_3 production is clearly due to HO_2 and CH_3O_2. The largest single source of HO_2 was the reaction of OH with CO, which accounted for 48% of the total HO_2 production at 20 m and 1300 EDT and nearly 60% of the total HO_2 production at 850 m and 1300 EDT. Methane oxidation accounted for 68% of the CH_3O_2 radical and 18% of the HO_2 at the 20 m grid point and 1300 EDT, while at 850 m methane oxidation was responsible for the production of 74% of the CH_3O_2 and 22% of the HO_2 at 1300 EDT. Isoprene oxidation, reflecting the strong height dependence of the isoprene concentration, accounted for 13% of the HO_2 production at 20 m, and only 2% of the HO_2 at 850 m. For the 20 m point isoprene is quite clearly the dominant non-methane hydrocarbon (NMHC) O_3 source followed by our generic alkane. At 850 m within the model the contribution to O_3 production by isoprene, relative to other non-methane hydrocarbons, is much less. This effect is due to the strong vertical gradient of isoprene concentrations calculated by the model. The effect of isoprene on the local photochemical production of O_3 at greater heights is further minimized by the near total depletion of isoprene within the boundary layer overnight by reaction with O_3 and NO_3. Isoprene does not begin to appreciably participate in the oxidation of NO, at 850 m within the model, until fresh emissions of isoprene reach that height with the growth of the boundary layer through the morning. A similar effect can be seen for all levels above the height of the

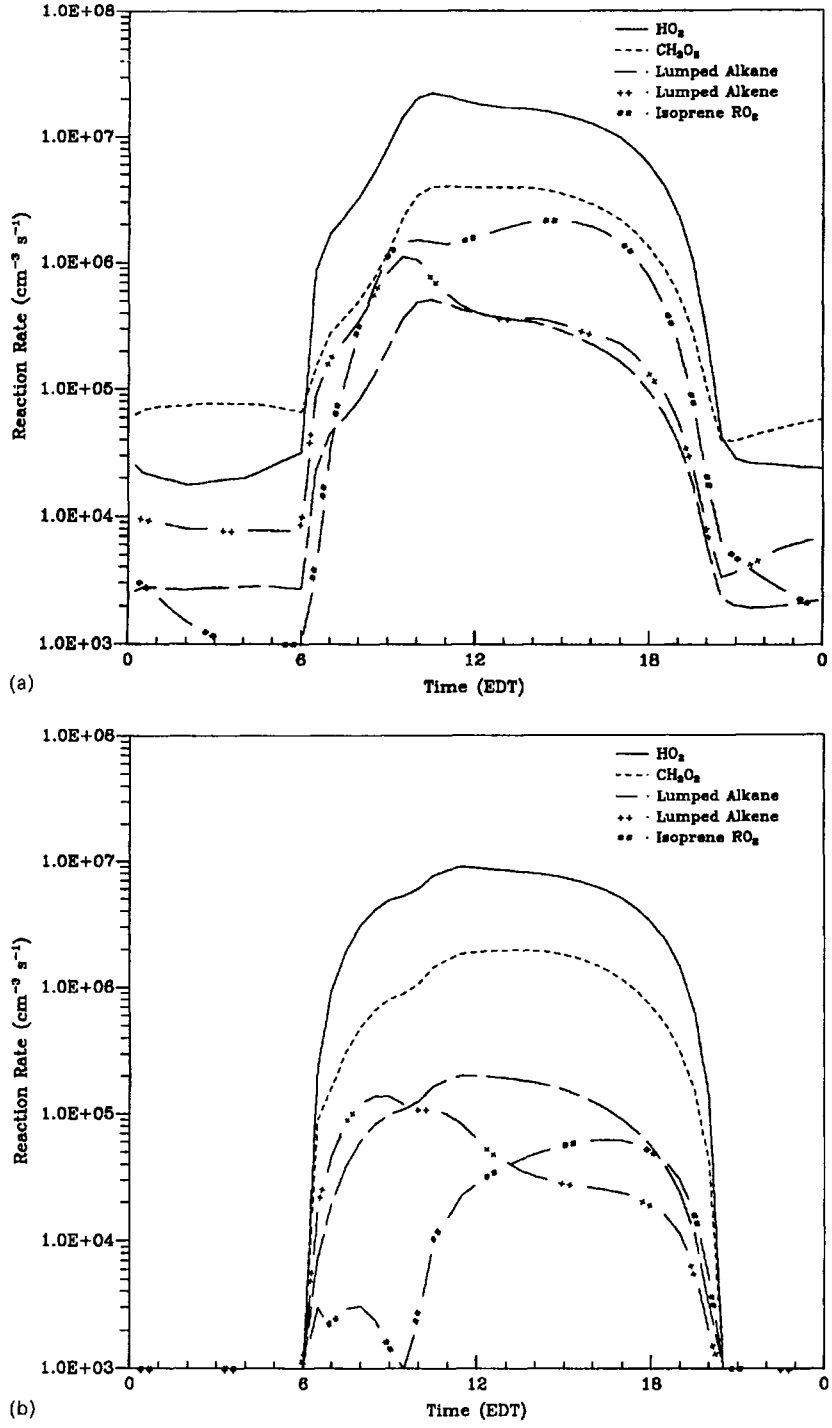

Fig. 7. Ozone production rates from NO + HO_2 and NO + RO_2 for CH_4 and several NMHC species at (a) 20 m and (b) 850 m.

NBL. Even accounting for the strong vertical gradient in isoprene concentrations, and the fact that observed concentrations of isoprene at the surface did not exceed 0.3 ppb on this day, isoprene was still important to the production of O_3 at the Hastings site. The amount of O_3 generation during the day in the mixed layer was calculated to be ~ 10 ppb.

For the case modelled here O_3 production is strongly NO_x limited. Model simulations performed with varying isoprene fluxes resulted in little variation in the total amount of O_3 produced during the day. Increasing the isoprene flux by up to a factor of 20 resulted in only a 1 ppb increase in the O_3 concentration predicted by the model for the grid point at 11 m and 1700 EDT. However, increasing the anthropogenic component of the NO_x flux by a factor of eight, while keeping the soil NO_x flux constant, resulted in a 10 ppb increase in the O_3 concentration at 11 m and 1700 EDT. A further increase in the NO_x flux gave decreasing O_3 concentrations.

Calculation of dO_3/dNO_x (Liu *et al.*, 1987), or the NO_x chain length, for the model run show that, for the NO_x levels used within the model, 26.6 molecules of O_3 should be produced for each NO_x molecule introduced. The NO_x chain length calculated by Hastie *et al.* (1994) predicts approximately 12 ozone molecules to be produced for each NO_x molecule consumed. The model NO_x chain length is more than twice as large as that given by the measurements.

Peroxyacetylnitrate

Peroxyacetylnitrate, PAN, concentrations are influenced by the equilibrium between the forward production reaction and the reverse thermal decomposition reaction,

$$CH_3COO_2 + NO_2 \rightleftharpoons PAN \qquad (6)$$

As such, the concentration of PAN will depend on the availability of the acetylperoxy radical, a product of NMHC oxidation, and NO_2. The rate at which PAN undergoes thermal decomposition is strongly temperature dependent (Hendry and Kenley, 1977) and at the midday temperatures encountered during 6 August, PAN will have a lifetime on the order of one hour. As such, PAN should reflect the effects of local chemistry.

The initial concentration of PAN was taken from the end of the five-day initialization run and agrees well with typical background PAN concentrations observed at Hastings. Concentrations of PAN are observed to rise rapidly after 900 EDT as the nocturnal inversion lifts and PAN from aloft mixes down (Fig. 8). During the time PAN is being mixed down from aloft, the rise in PAN concentration calculated by the model lags that shown in the observations. This lag may indicate that during the nighttime, the model is underpredicting the PAN concentrations above the NBL. By the time the PBL is fully developed the model PAN and observations show good agreement. There is a large increase in PAN concentrations through the late afternoon hours, after photochemical activity has decreased. The late afternoon rise in PAN, like that of ozone, is most likely related to transport (Hastie *et al.*, 1994).

Peroxy radicals

Figure 9a shows a comparison of the sum of HO_2 and RO_2 radicals calculated by the model and the RO_x ($HO_2 + RO_2$) measurements of Arias *et al.* (1994) made using a chemical amplifier technique. There is substantial disagreement between the model results and measurements. It is believed that peroxy radical concentrations can be significantly affected by the destruction of HO_2 by heterogeneous reactions (Schwartz, 1984; Ross and Noone, 1991). Model runs were conducted which included an HO_2 loss reaction with a first-order rate constant. The idea was to mimic the process of HO_2 loss on particles and derive an estimate of the rate at which the heterogeneous reaction must occur to significantly affect peroxy radical concentrations. Without a first-order loss for HO_2, the model predicts a peak peroxy radical concentration of 42 ppt, while observations show a maximum RO_x concentration of 17 ppt. A first-order rate constant for the HO_2 loss of 2.0×10^{-2} s^{-1} was necessary to suppress peak peroxy radical concentrations to approximately 20 ppt. If the peroxy radical concentrations are being suppressed by heterogeneous reaction, and were as low as measurements indicated, the amount of O_3 photochemically generated at the site would be much less than that calculated by the model. In such a case, a large fraction of the increase in ozone concentration observed on 6 August can only be explained by the photochemical production of ozone elsewhere, followed by transport to the Hastings site.

More information about the peroxy radical concentration may be derived from the NO_2/NO ratio, since the concentration of peroxy radicals will influence the partitioning of NO_x between NO and NO_2. Figure 9b shows the model calculations and observations for the NO_2/NO ratio. The model calculations for the NO_2/NO ratio show a large degree of agreement with the observed NO_2/NO ratio. As explained above, NO_2 and NO form a fast photochemical system during daylight periods, where the photolysis of NO_2 to NO is balanced by the conversion of NO back to NO_2 by reaction with O_3 and peroxy radicals. As such, the ratio of NO_2 to NO will be dependent upon the NO_2 photolysis rate, the ozone concentration, and the peroxy radical concentration. Based on the model calculation for the NO_2 photolysis rate, the NO_2/NO ratio would have been approximately 1.5, if there had been no effects from peroxy radicals, while the midday NO_2/NO ratio calculated by the model was closer to 2.1. As can be seen, the expected effect of peroxy radicals on the NO_2/NO ratio will be small, and given the error and scatter in the measured NO_2/NO ratio, and the expected uncertainty in the photolysis rate for NO_2, the effect of peroxy radicals will not be significant. As a result, no definite conclusions can be reached about the modelled peroxy radical concentration,

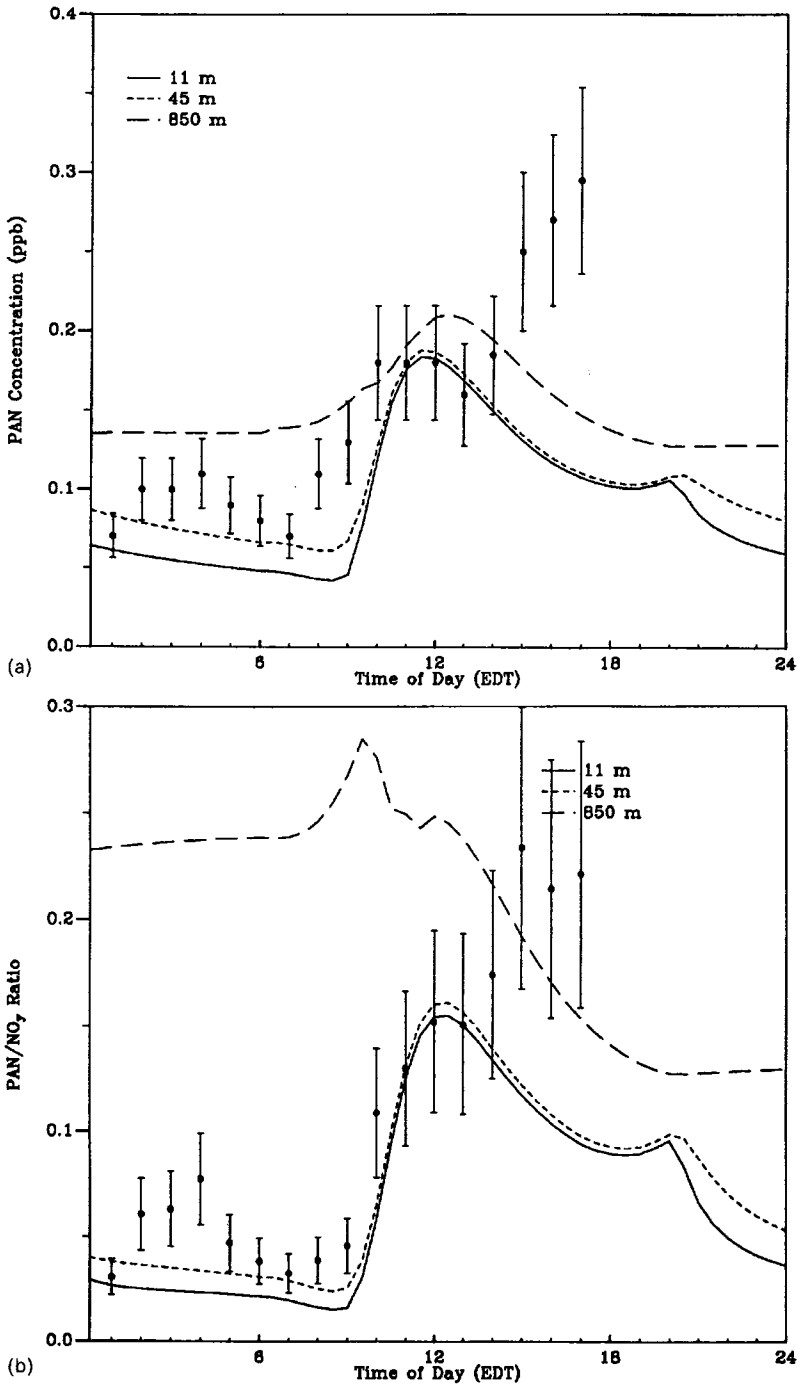

Fig. 8. (a) PAN model mixing ratios vs time at 11, 45, and 850 m are presented. Also shown are the surface PAN measurements (Shepson, 1993). (b) Model calculated PAN/NO_y ratio at 11, 45, and 850 m vs time and the surface measurements.

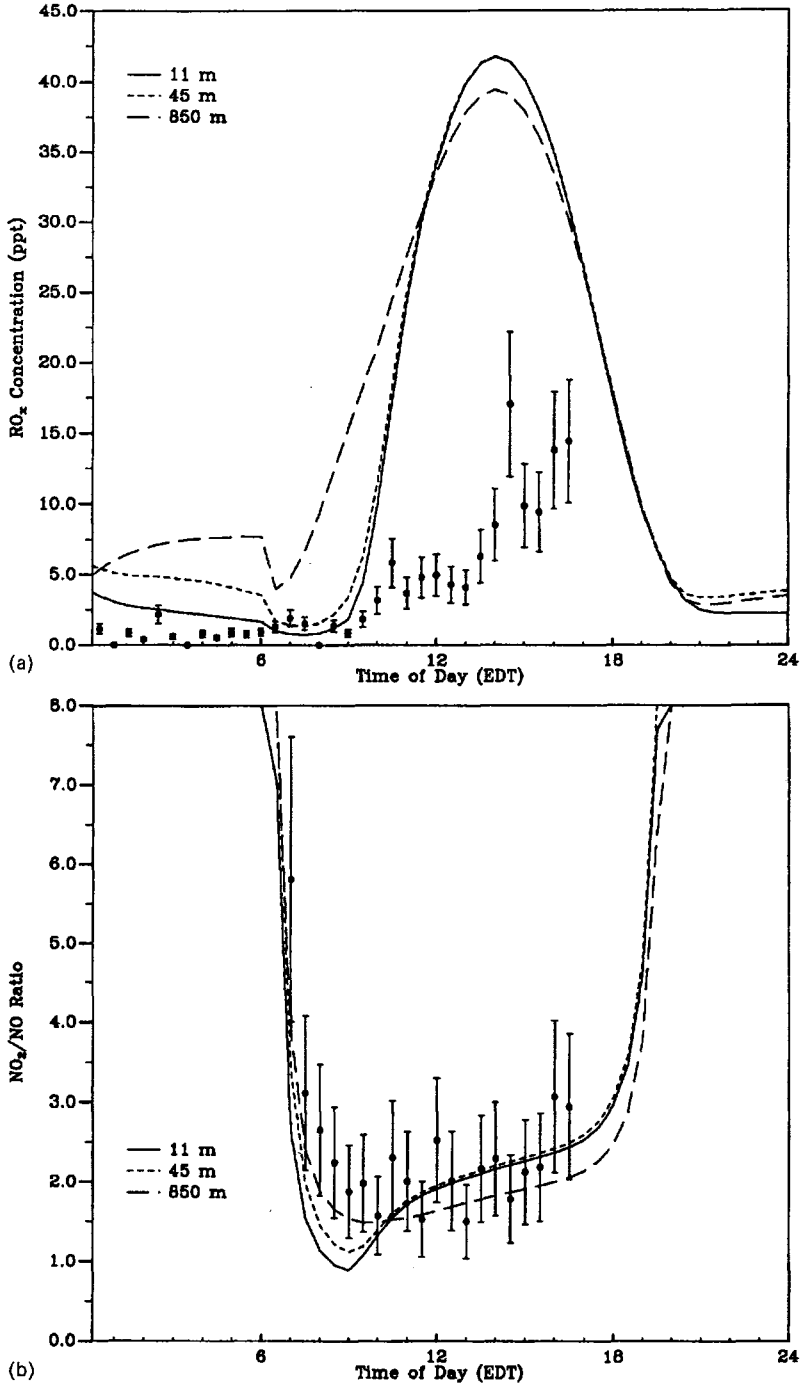

Fig. 9. (a) Model calculated ($HO_2 + RO_2$) mixing ratios at 11 m vs time. Also shown are the $RO_x = HO_2 + RO_2$ measurements of Arias *et al.* (1994). (b) The model calculations for the NO_2/NO ratio at 11, 45, and 850 m. Also shown are the surface observations of the NO_2/NO ratio (Hastie, 1993).

in relation to the actual peroxy radical concentration, from the NO_2/NO ratio.

At this point we cannot definitively account for the disparity between the measurements and the model results for the peroxy radical concentrations.

Non-methane hydrocarbons

Figure 10 compares the measurements (Niki, 1993) and calculations for C_2H_6, C_3H_8 and our generic alkane for several heights for the 6 August period. The C_2H_6 comparison shown in Fig. 10a is more by way of a consistency check since the C_2H_6 chemical time constant is much greater than one day. It is only the period around 6 a.m. that suggests a signature of a local C_2H_6 source. The C_3H_8 comparison shown in Fig. 10b is more problematical: the model suggests that we should not expect a substantial signature due to local sources except perhaps in the early morning before the NBL breaks up. In addition, given that the site may be coming under the influence of more polluted air later in the day (cf. the C_2Cl_4 measurements in Fig. 1 of Reid *et al.*, 1994), we might expect the C_3H_8 to be increasing with time. In fact, the measurements indicate C_3H_8 decreasing with time. Possibly, the air from the west may have sampled a C_3H_8 source or there may be problems with the C_3H_8 measurements. The disparity between the model and measurements will not seriously impact O_3 or radical generation. To compare our generic alkane model results shown in Fig. 10c we have added the C_4 and higher alkanes from Niki (1993). The results indicate a reasonable agreement between the measurements and model, except for what appears to be a local pollution spike that registers in the $C_{\geq 4}$ alkanes and propene but not in ethane, propane or ethene.

The chemical time constants for the alkenes are such that any alkenes originating from Toronto will be oxidized before reaching the Hastings site. Thus, a comparison of the measured alkenes with the model results should be more indicative of local sources than is the case for the alkanes. Figure 11 shows the model results for several heights for C_2H_4 (panel a) and our generic (propene-like) alkene (panel b). As noted earlier the lumped alkene emissions have been adjusted to give better agreement with the measurements. Nevertheless, the temporal agreement for C_2H_4 is good and certainly suggests that there is substantial local emission. The comparison of the measurements with our generic alkene shown in Fig. 11b suggests that our alkene source is still too small by at least a factor of two, in spite of the enhanced source ratio noted in the previous emission section.

An important radical generator with a potential local impact is HCHO. Figure 12 shows the measurements (Hastie, 1993) and the model mixing ratios. The

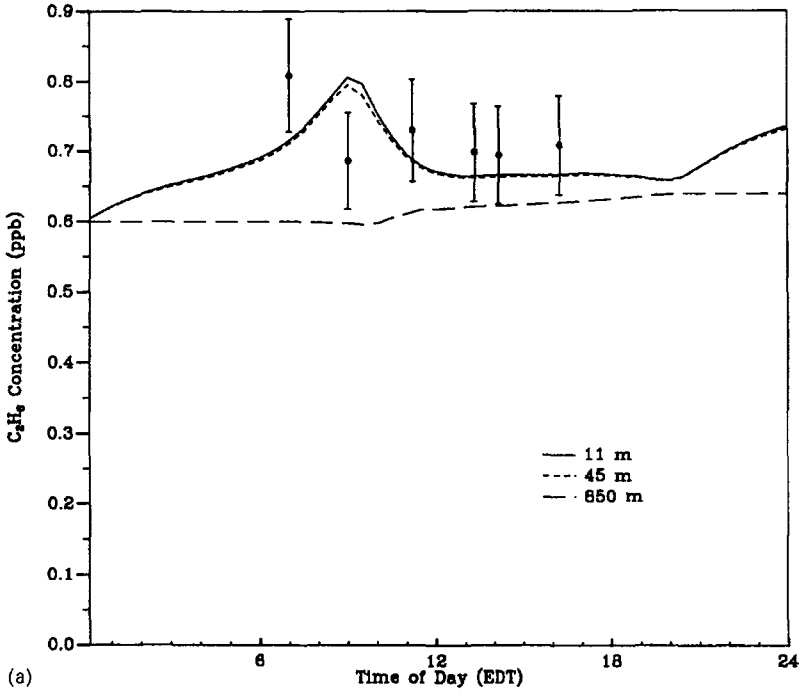

Fig. 10a.

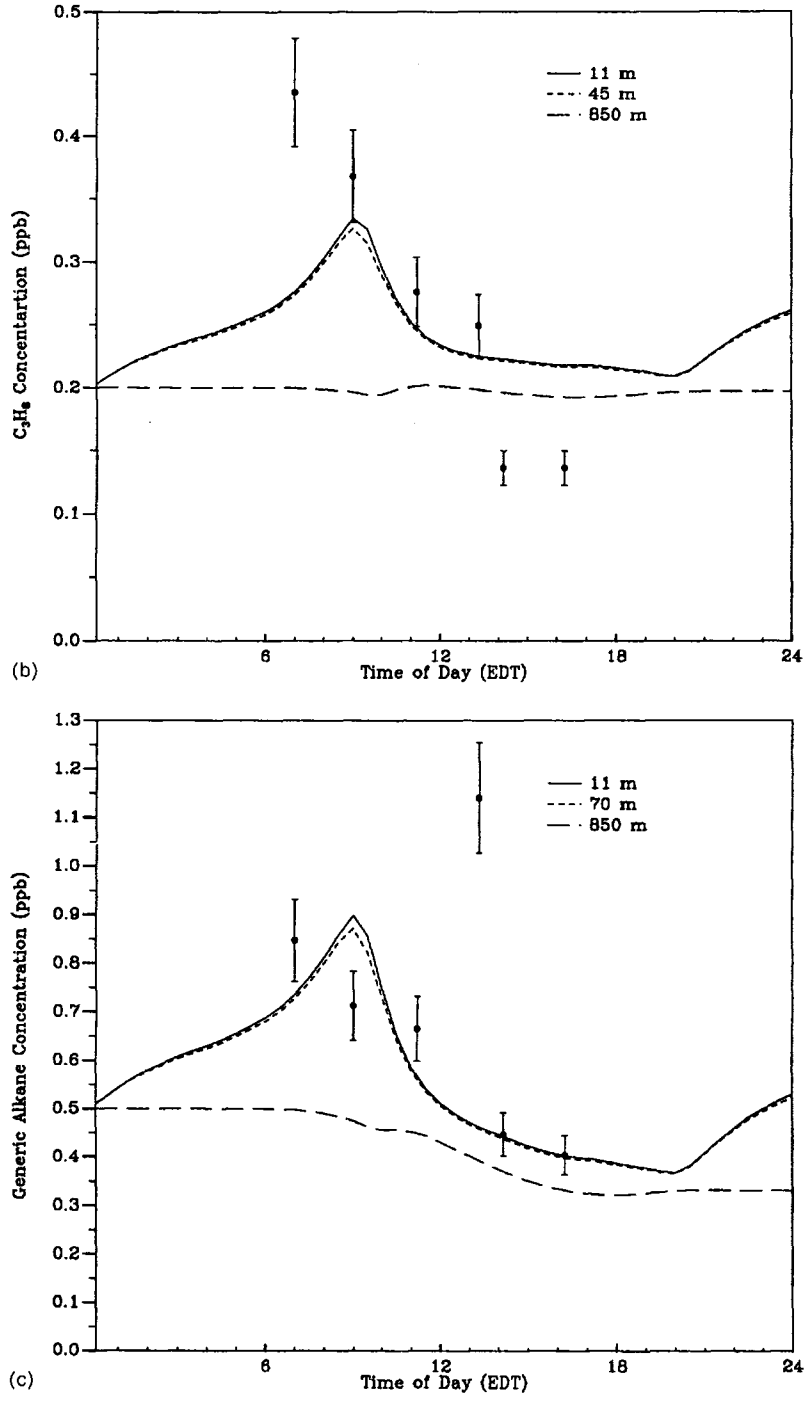

Fig. 10. Alkane mixing ratios vs time for 2 altitudes, 11 and 850 m. (a) C_2H_6, (b) C_3H_8 and (c) generic alkane. The measurements from Niki (1993) are also shown.

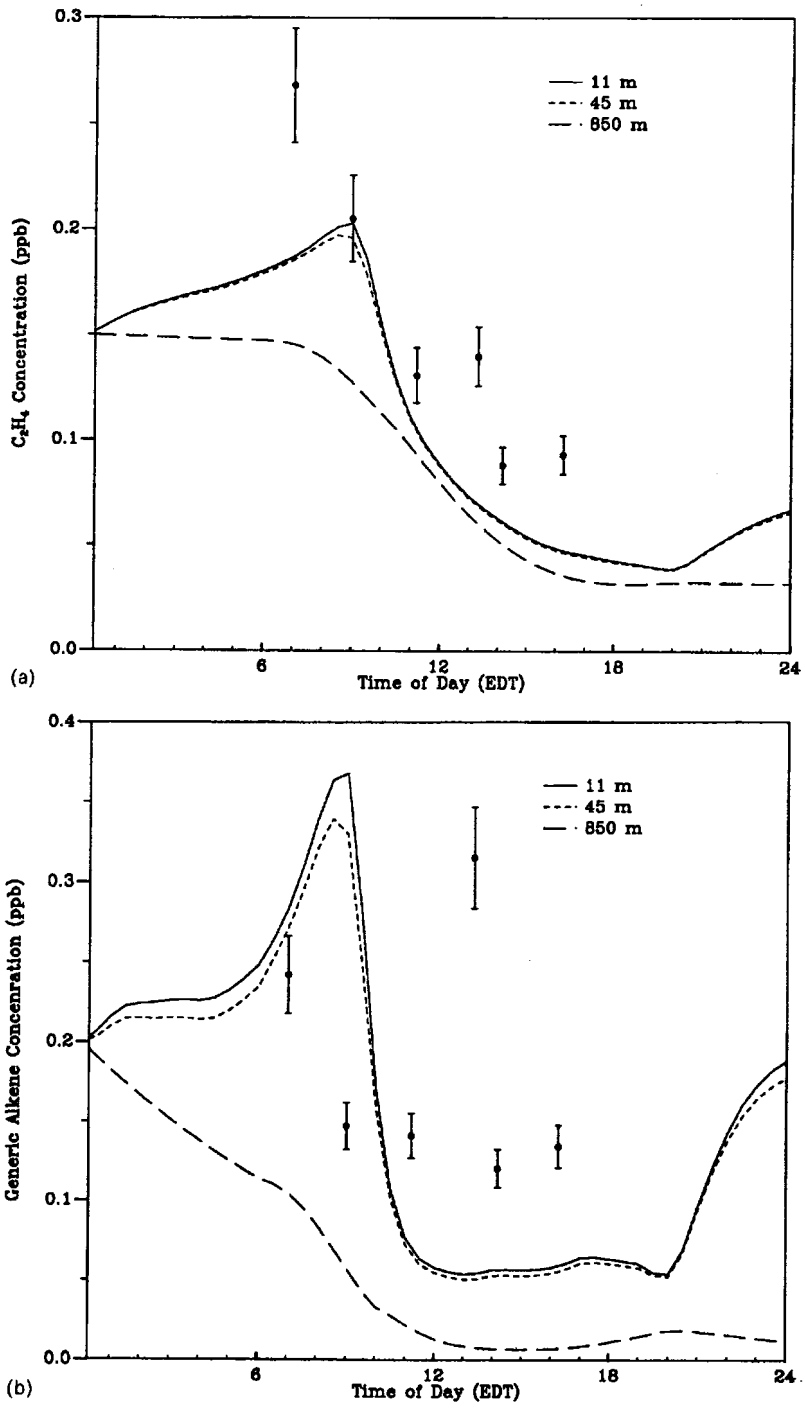

Fig. 11. Alkene mixing ratios vs times for 11 and 850 m. (a) C_2H_4 and (b) generic alkene. The measurements from Niki (1993) are also shown.

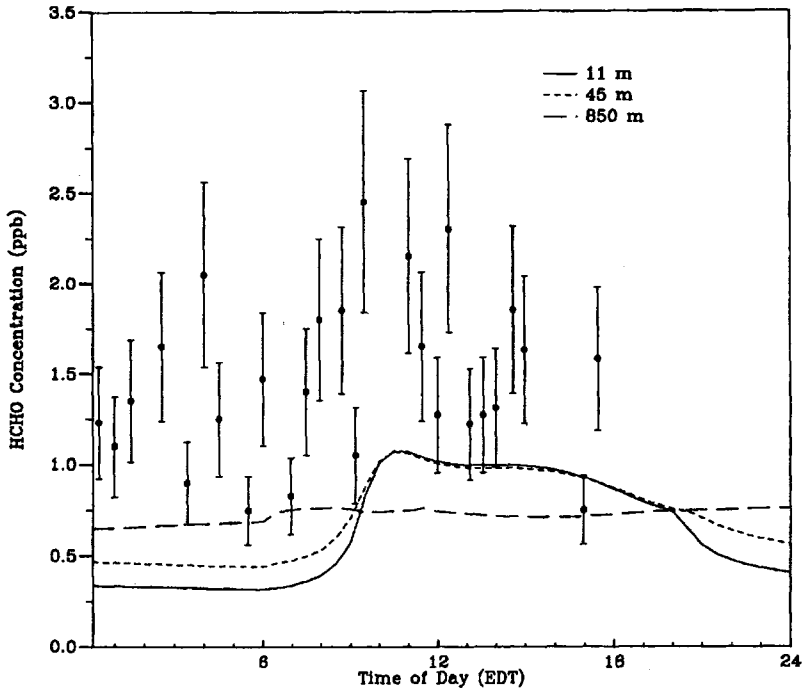

Fig. 12. Formaldehyde mixing ratios vs times for 11, 45, and 850 m. The surface measurements of Hastie (1993) are also shown.

observations are quite noisy and the mean value appears to be about a factor of two larger than the model results, although the model results are just within a standard deviation. The nighttime model results indicate the effects of deposition, but ameliorated by generation of HCHO via NO_3 reactions. The effects of deposition are not apparent in the measurements.

As discussed above organic nitrates may represent a significant fraction of the total reactive nitrogen. Our modelling results indicate a production of 35 ppt of nitrates from C_3H_8, the model lumped alkane, and the lumped alkene over the course of the day. This compares with the measurements of the corresponding organic nitrates which indicate between 10 and 20 ppt nitrates. The lumped alkane accounts for approximately 26 ppt of the above nitrates and, while the models over-prediction of organic nitrates may indicate an overestimation of hydrocarbon oxidation, the discrepancy most probably arises as a result of attempting to assign a single nitrate yield to a lumped hydrocarbon species. In addition to the above nitrates, the model also predicts the production of 34 ppt of organic nitrates from the OH reaction with isoprene, methyl vinyl ketone and methacrolein, where nearly 60% of these are in the form of isoprene nitrate. Overall organic nitrates are predicted to account for 5.9% of the total reactive nitrogen by the end of the model run.

SUMMARY

This paper presents a comparison between measurements and a one-dimensional model at the Hastings site for relatively unpolluted background conditions. There is agreement between many of the key trace gas observations made at the Hastings site on 6 August 1992 and the model calculations presented here. The model calculates 10 ppb of net local ozone production during the course of the day which agrees with observations, though after 1500 EDT the advection of ozone produced elsewhere appears to have an influence on ozone concentrations at the site. For the background conditions, methane plays a major role in the production of ozone, although among the NMHCs isoprene plays an important role near the surface. Since the photochemical production of ozone is strongly limited by the availability of NO_x, local anthropogenic and biogenic sources are important and have been shown to strongly influence the local chemistry.

The modelling suggests that there are local sources of alkenes and NO_x and that there are likely nocturnal emissions of NO_x that are certainly similar in magnitude to measured soil emissions. However, the measured RO_2 mixing ratios are more than a factor of two less than the noon-time model values and, as yet, we have no explanation, though heterogeneous reactions may be responsible.

As evidenced by observations, the transport of polluted air masses, possibly influenced by lake breezes, will occasionally affect the Hastings site. A more detailed study of this effect using a three-dimensional model is in progress.

Acknowledgements—This is Scientific Contribution number 94-10 of the Canadian Institute for Research in Atmospheric Chemistry (CIRAC). The work described herein was undertaken as part of the CIRAC SONTOS project.

The authors wish to thank the Ontario Ministry of the Environment for support through a RAC grant, the Natural Science and Engineering Research Council of Canada, and the Atmospheric Environment Service of Canada for continuing support. We also wish to thank Drs X. Lin and P. Taylor for useful discussions, and the reviewers of the paper for their input.

REFERENCES

Arias M. C., Mozurkewich M. and Hastie D. R. (1994) Personal communication.

Atkinson R. (1990) Gas-phase tropospheric chemistry of organic compounds: a review. *Atmospheric Environment* **24,** 1–41.

Buhr M. P., Parrish D. D., Norton R. B., Fehsenfeld F. C., Sievers R. E. and Roberts J.M. (1990) Contribution of organic nitrates to the total reactive nitrogen budget at a rural eastern U.S. site. *J. geophys. Res.* **95,** 9809–9816.

Carter W. P. L. and Atkinson R. (1989) Alkyl nitrate formation from the atmospheric photooxidation of alkanes: a revised estimation method. *J. atmos. Chem.* **8,** 165–173.

CCME (1991) Canadian Council of Ministers of the Environment Management Plan for Nitrogen Oxides (NO_x) and Volatile Organic Compounds (VOCs).

Crosley D. R. (1994) *Issues in the Measurement of Reactive Nitrogen Compounds in the Atmosphere.* SRI International Report MP 94-035, Menlo Park, CA.

Fahey D. W., Hubler W. G., Parris D. D., Williams E. J., Norton R. B., Ridley B. A., Singh H. B., Liu S. C. and Fehsenfeld F. C. (1986) Reactive nitrogen species in the troposphere: measurements of NO, NO_2, HNO_3, particulate nitrate, peroxyacetyl nitrate (PAN), O_3, and total reactive nitrogen (NO_y) at Niwot Ridge, Colorado. *J. geophys. Res.* **91,** 9781–9793.

Guenther A. B., Zimmerman P. R., Harley P. C., Monson R. K. and Fall R. (1993) Isoprene and monoterpene emission rate variability: model evaluations and sensitivity analysis. *J. geophys. Res.* **98,** 12,609–12,617.

Hastie D. R. (1993) Personal communication.

Hastie D. R., Shepson P. B., Sharma S. and Schiff H. I. (1993) The influence of the nocturnal boundary layer on a secondary trace species in the atmosphere at Dorset, Ontario. *Atmospheric Environment* **27A,** 533–541.

Hastie D. R., Shepson P. B., Roussel P., Lazlo S. and Melo O. (1994) Summertime NO_x, NO_y, and ozone at a site in rural Ontario. *Atmospheric Environment* **30,** 2157–2165.

Heck W. W., Cure W. W., Rawlings J. O, Zaragoza L. J., Heagle A. S., Heggestad H. E., Kohut R. J., Kress L. W. and Temple P. J. (1984) Assessing impacts of ozone on agricultural crops, II, Crop yield functions and alternative exposure statistics. *J. Air Pollut. Control Ass.* **34,** 810–817.

Heck W. W., Taylor O. C. and Tingey D. T. (1988) Assessment of crop loss from air pollutants. In *Proc. Int. Conf. on the National Crop Loss Assessment Network (NCLAN).* Elsevier, New York.

Henderson G. S., McConnell J. C. and Evans W. F. J. (1990) Model studies of the oxidation of light hydrocarbons in the troposphere and stratosphere. *Atmos-Oceans* **28,** 48–89.

Hendry D. G. and Kenley R. A. (1977) Generation of peroxy radicals from peroxy nitrates (RO_2NO_2). Decomposition of peroxyacyl nitrates. *J. Am. Chem. Soc.* **99,** 3198.

Jacob D. J. and Wofsy S. C. (1988) Photochemistry of biogenic emissions over the amazon forest. *J. geophys. Res.* **93,** 1477–1486.

Liu S. C., Trainer M., Fehsenfeld F., Parrish D. D., Williams E. J., Fahey D. W., Hubler G. and Murphy P. C. (1987) Ozone production in the rural troposphere and the implications for regional and global ozone distribution. *J. geophys. Res.* **92,** 4191–4207.

Lurmann F. W., Lloyd A. C. and Nitta B. (1983) Modelling potential ozone impacts from natural hydrocarbons, 2, hypothetical biogenic HC emission scenario modelling. *Atmospheric Environment* **17,** 1951–1963.

Lurmann F. W., Lloyd A. C. and Atkinson R. (1986) A chemical mechanism for use in long-range transport/acid deposition computer modelling. *J. geophys. Res.* **91,** 10,905–10,936.

McConnell J. C., Evans W. F. J. and Templeton E. M. J (1991) Model simulation of chemical depletion of arctic ozone during the winter of 1989. *J. geophys. Res.* **96,** 10,930–10,933.

McLaren R., Singleton D. L., Lai J., Wu Z. and Niki H. (1994) Analysis of emission sources contributing to ambient hydrocarbon distributions measured at urban sites in Toronto. *Atmospheric Environment* **30,** 2219–2232.

MOE (1989) *Impact of Ozone Exposure on Vegetation in Ontario.* Ontario Ministry of the Environment.

Niki H. (1993) Personal communication.

O'Brien J. M., Shepson P., Muthuramu K., Hao C., Niki H., Taylor R. and Roussel P. (1995) Measurements of multifunctional organic nitrates and their contribution to NO_y during the Southern Ontario Oxidant Study (SONTOS), *J. geophys. Res.* (submitted).

Parrish D. D., Trainer M., Williams E. J., Fahey D. W., Hubler G., Eubank C. S., Liu S. C., Murphy P. C., Albritton D. L. and Fehsenfeld F. C. (1986) Measurements of the NO_x–O_3 photostationary state at Niwot Ridge, Colorado. *J. geophys. Res.* **91,** 5361–5370.

Reid N. W., Niki H., Hastie D. R., Shepson P., Roussel P., Melo O., Mackay G., Drummond J., Schiff H. I., Poissant L. and Moroz W. (1994) The Southern Ontario Oxidant Study (SONTOS): overview and case studies for 1992. *Atmospheric Environment* **30,** 2125–2132.

Ross H. B. and Noone K. J. (1991) A numerical investigation of the destruction of peroxy radical by Cu ion catalysed reactions on atmospheric particles. *J. atmos. Chem.* **12,** 121–136.

Roussel P. and Moroz W. J. (1992) Oxidant monitoring in southern Ontario: The suitability of a site near Hastings, Ontario, as a rural monitoring station within the Windsor–Quebec City corridor. Report No. 92-109-K, Ontario Hydro Research Division, Toronto ON.

Roussel P., Lin X., Camacho F., Laszlo S., Taylor R., Melo O. and Niki H. (1994) Observation of O_3 and precursor levels at two sites around Toronto, Ontario, during the summer of 1992. *Atmospheric Environment* **30,** 2145–2155.

Schwartz S. E. (1984) Gas- and aqueous-phase chemistry of HO_2 in liquid water clouds. *J. geophys. Res.* **89,** 11,589–11,598.

Shepherd M. F., Barzetti S. and Hastie D. R. (1991) The production of atmospheric NO_x and N_2O from a fertilized

agricultural soil. *Atmospheric Environment* **25A,** 1961–1969.

Shepson P. (1993) Personal communication.

Singh M. P., McNider R. T. and Lin J. T. (1993) An analytical study of diurnal wind variations in the boundary layer and the low level nocturnal jet. *Boundary-Layer Met.* **63,** 397–423.

Stull R. B. (1988) *An Introduction to Boundary Layer Meteorology.* Kluwer, Boston.

Taylor O. C. (1969) Importance of peroxyacetyl nitrate (PAN) as a phytotoxic air pollutant. *J. Air. Pollut. Control Ass.* **19,** 347–351.

Trainer M., Hsie Y., McKeen S. A., Tallamraju R., Parrish D.D., Fehsenfeld F.C. and Liu S.C. (1987) Impact of natural hydrocarbons on hydroxyl and peroxy radicals at a remote site. *J. geophys. Res.* **92,** 11,879–11,894.

Tuazon E. C. and Atkinson R. (1990) A product study of the gas-phase reaction of isoprene with the OH radical in the presence of NO_x. *Int. J. Chem. Kinet.* **14,** 1221–1236.

Wong S. (1993) Ontario Ministry of the Environment, personal communication.